

Probing Cosmic Background Dynamics with a Cosmological-model-independent Method

Yang Liu,¹★ Bao Wang,^{2,3}† Hongwei Yu^{1,4}‡ and Puxun Wu^{1,4}§

¹Department of Physics and Synergetic Innovation Center for Quantum Effects and Applications, Hunan Normal University, Changsha, Hunan 410081, China

²School of Astronomy and Space Sciences, University of Science and Technology of China, Hefei 230026, China

³Purple Mountain Observatory, Chinese Academy of Sciences, Nanjing 210023, China

⁴Institute of Interdisciplinary Studies, Hunan Normal University, Changsha, Hunan 410081, China

26 July 2024

ABSTRACT

The Hubble constant H_0 tension has emerged as the most serious crisis in modern cosmology, potentially indicating that the Λ CDM model may not describe our universe accurately. In this paper, we establish a new, cosmological-model-independent method to study the cosmic background dynamics. Using the latest Pantheon+ Type Ia supernova (SN Ia) sample and the model-independent SN Ia sample (P+1690), we derive values for the luminosity distance, the Hubble parameter, and the deceleration parameter at five different redshift points ranging from 0.12 to 0.52. Our analysis shows that results obtained from the Pantheon+ sample align with the predictions of the Λ CDM model within 2σ confidence level (CL), while those obtained from the P+1690 sample exhibit deviations of about $2 \sim 3\sigma$ CL. Furthermore, we explore the equation of state (EoS) of dark energy and find that while the EoS values from the Pantheon+ sample remain consistent with -1 within 2σ CL, the P+1690 sample does not conform to this standard. These findings remain unchanged after the inclusion of the Hubble parameter measurements in our analysis. Our results indicate that the Λ CDM model remains compatible with the Pantheon+ SN Ia and the Hubble parameter measurements at 2σ CL.

Key words: (*cosmology:*) cosmological parameters – cosmology: observations

1 INTRODUCTION

The cosmological constant Λ plus cold dark matter (Λ CDM) is the simplest and most favored cosmological model to describe the cosmic evolution. The Λ CDM model, although fits observational data very well, still faces some challenges. Among them, the Hubble constant (H_0) tension is the most notable one and it has been considered as the most serious crisis in modern cosmology (Riess 2020; Perivolaropoulos & Skara 2022; Tully 2023; Liu et al. 2023, 2024). The H_0 tension refers to the discrepancy (more than 5σ) between the measurements of H_0 using the near type Ia supernova (SN Ia) calibrated by Cepheids (Riess et al. 2022) and that from the high-redshift cosmic microwave background (CMB) radiation observation within the framework of the Λ CDM model (Planck Collaboration 2020a), and it indicates that the assumed Λ CDM model used to determine the Hubble constant may be inconsistent with our present Universe or there may be potentially unknown systematic errors in the observational data. It is worth noting, however, that any systematics, which could explain the H_0 tension, have not been found (Efstathiou 2014; Feeney et al. 2018; Riess et al. 2016; Cardona et al. 2017; Zhang et al. 2017; Follin & Knox 2018; Riess et al. 2018a,b). Thus,

it is necessary to investigate whether the Λ CDM model can correctly describe our Universe.

The cosmological constant as dark energy has a constant equation of state (EoS) parameter w_{DE} equal to -1 , where w_{DE} is defined as $w_{\text{DE}} \equiv \frac{P_{\text{DE}}}{\rho_{\text{DE}}}$ with P_{DE} and ρ_{DE} being the pressure and energy density of dark energy, respectively. Thus, generalizing the EoS of dark energy from -1 to an arbitrary constant w_{DE} or a parametrized form as a function of redshift z , e.g., the Chevallier-Polarski-Linder (CPL) parameterization (Chevallier & Polarski 2001; Linder 2003) with $w_{\text{DE}}(z) = w_0 + w_a z / (1 + z)$, and constraining w_{DE} or the coefficients in the parameterization from observational data, we can judge the viability of the cosmological constant as dark energy by analyzing whether $w_{\text{DE}} = -1$ is allowed by the observations (Liu et al. 2008; Demianski et al. 2020). Recently, by combining the baryon acoustic oscillation from the first year of observations from the Dark Energy Spectroscopic Instrument (DESI) (DESI Collaboration 2024) with CMB anisotropies from Planck (Planck Collaboration 2020a,b) and CMB lensing data from Planck and Atacama Cosmology Telescope (Carron et al. 2022; Qu et al. 2024), and DES-SN5YR supernova datasets (Abbott et al. 2024), DESI Collaboration (2024) found that the time-varying dark energy EoS parametrized by the CPL model is more favored than $w_{\text{DE}} = -1$ with a statistical significance of 3.9σ .

Reconstructing the cosmic background evolution directly from the observations is a more reliable method to understand the expanding history of our Universe. The usual methods include the nonparametric

★ yangl@hunnu.edu.cn

† baowang@pmo.ac.cn

‡ Corresponding author: hwyu@hunnu.edu.cn

§ Corresponding author: pxwu@hunnu.edu.cn

Bayesian reconstruction (Zhao et al. 2012, 2017) and the Gaussian process (Holsclaw et al. 2010; Seikel et al. 2012; Shafieloo et al. 2012). Using the observational data, e.g., SN Ia, one can reconstruct the Hubble parameter ($H(z)$) or the luminosity distance ($d_L(z)$) with their derivatives, and then compare them with the predictions from the Λ CDM model to determine whether the Λ CDM model can correctly describe the cosmic evolution. However, when reconstructing cosmic evolution in low (high) redshift regions, high (low) redshift observational data are utilized concurrently. Consequently, the low (high) redshift data influence the reconstructed results for the high (low) redshift regions.

In this work, we establish a new method to obtain the cosmic background dynamics in different redshift regions from observational data. In our method, we only assume the cosmological principle, which implies that the universe can be described using the Friedmann-Lemaître-Robertson-Walker (FLRW) metric. Therefore, our approach is metric-dependent. However, it does not necessitate the assumption of any specific energy components within the universe, and in this sense, our method is cosmological-model-independent. Furthermore, when the properties of the cosmic expansion are studied at a given redshift, the observational data in the near region of this redshift point rather than the full data will be used. From the Pantheon+ SN Ia and the Hubble parameter measurements, we obtain the values of the Hubble parameter and the deceleration parameter at different redshifts, and find that they are consistent with the predictions of the Λ CDM model at 2σ confidence level (CL).

2 METHOD

For a homogeneous and isotropic Universe described by the FLRW metric, the Hubble parameter H , which gives the cosmic expanding velocity, is defined as

$$H \equiv \frac{1}{a} \frac{da}{dt}, \quad (1)$$

where a is the cosmic scale factor and t the cosmic time. In a spatially flat Λ CDM model, the Hubble parameter has the form: $H(z) = H_0 \sqrt{\Omega_{m0}(1+z)^3 + (1-\Omega_{m0})}$ with Ω_{m0} being the present matter density parameter. Using the Hubble parameter, one can obtain the luminosity distance $d_L(z)$:

$$d_L(z) = (1+z) \int_0^z \frac{1}{H(z)} dz \quad (2)$$

in a spatially flat universe, where the velocity of light is set to 1. Comparing the theoretical value and the observational one of the luminosity distance can yield constraints on the cosmological parameters, i.e. Ω_{m0} , after choosing a concrete cosmological model. To cosmological-model-independently understand the cosmic dynamics, we perform the Taylor expansion of the luminosity distance at a given redshift z_i and then obtain:

$$d_L(z) = d_{L,i} + (z - z_i) \left(\frac{1+z_i}{H_i} + \frac{d_{L,i}}{1+z_i} \right) + (z - z_i)^2 \left(\frac{1}{H_i} - \frac{1+q_i}{2H_i} \right) + \mathcal{O}((z - z_i)^3), \quad (3)$$

where $H_i = H(z_i)$, $d_{L,i} = d_L(z_i)$, and $q_i = q(z_i)$ with $q \equiv -\frac{1}{aH^2} \frac{d^2a}{dt^2}$ being the cosmic deceleration parameter, are three free parameters. If we can determine their values from the observational data, the cosmic dynamics will be known. Since the convergence region of the Taylor series of the luminosity distance and the Hubble parameter is the near region around $z = z_i$, we only consider the

observational data in the redshift region $|z - z_i| \leq \Delta z$ to constrain $d_{L,i}$, H_i and q_i , where Δz represents the convergence radius. When $z_i = 0$, our method reduces to the usual cosmographic one, which has been widely used to study the cosmic expanding history (Visser 2005; Luongo 2011; Aviles et al. 2012; Dunsby & Luongo 2016; Capozziello et al. 2019, 2020; Mehrabi & Rezaei 2021; Gao et al. 2023; Zhang et al. 2023).

Once the constraints on H_i and q_i at a given redshift are obtained, we can calculate the EoS parameter of dark energy $w_{DE,i}$ at that redshift

$$w_{DE,i} = \frac{H_i^2(1-2q_i)}{3 \left[H_0^2 \Omega_{m0}(1+z_i)^3 - H_i^2 \right]} \quad (4)$$

after assuming that the energy component of the Universe consists of pressureless matter and dark energy and the Universe is spatially flat.

3 SAMPLES AND RESULTS

3.1 Pantheon+ SN Ia

The latest Pantheon+ SN Ia sample (Scolnic et al. 2022) will be used firstly to constrain parameters $d_{L,i}$, H_i , and q_i , which includes 1701 light-curves of 1550 distinct SN Ia. The allowed regions for the parameters $d_{L,i}$, H_i , and q_i can be determined using the Markov Chain Monte Carlo (MCMC) method to minimize the χ_{SN}^2 , expressed as:

$$\chi_{SN}^2 = \hat{Q}^\dagger C_{P+}^{-1} \hat{Q}, \quad (5)$$

where $\hat{Q} \equiv \hat{\mu}_{obs}^{corr} - \mu_{th}$, with $\hat{\mu}_{obs}^{corr}$ representing the array of observed corrected SN Ia distance modulus and μ_{th} being the corresponding theoretical values, and C_{P+} is the covariance matrix. The corrected SN Ia distance modulus are obtained from (Tripp 1998; Brout et al. 2022)

$$\mu_{obs}^{corr} = m_B - M_B + \alpha x_1 - \beta c + \delta_{host} - \delta_{bias}, \quad (6)$$

where m_B is the apparent magnitude in the B-band filter, which is related to the SALT2 light-curve amplitude x_0 by $m_B = -2.5 \log(x_0)$, x_1 is the stretch parameter, c is the light-curve color, α and β are coefficients relating luminosity to x_1 and c , respectively, M_B is the fiducial B-band absolute magnitude of SN Ia, δ_{host} accounts for host-galaxy mass luminosity correction, and δ_{bias} corrects for selection biases from simulations following (Brout & Scolnic 2021; Popovic et al. 2021). The value of μ_{th} can be derived from the luminosity distance:

$$\mu_{th}(z) = 25 + 5 \log(d_L(z)). \quad (7)$$

Given the high degeneracy between the Hubble parameter H_i and M_B , a Gaussian prior of -19.253 ± 0.027 mag is used for M_B when only SN Ia data are utilized. The covariance matrix in the Pantheon+ sample includes statistical (C_{stat}) and systematic (C_{sys}) components, addressing uncertainties from measurement errors, gravitational lensing, and peculiar-velocity effects. The redshift z used is the Hubble-diagram redshift z_{HD} , derived from the CMB frame redshift z_{CMB} with corrections for peculiar velocity.

For the Pantheon+ sample with z_{HD} , we exclude those data whose redshifts are less than 0.01 since the unmodeled peculiar velocities will strongly impact the nearby SN Ia sample (Brout et al. 2022). Before using these real data to constrain the free parameters, we need to check the reliability of our method. To do so, we mock the SN Ia data from the fiducial model to assess the impact of different

Δz ($\Delta z = 0.15$ and 0.12) on the results. The detailed discussions can be found in the Appendix A. The results indicate that when $\Delta z = 0.15$ is used, the parameter q_1 is consistent with the fiducial model only at the margin of 1σ CL, whereas it conforms well with the model when using $\Delta z = 0.12$. Thus, $\Delta z = 0.12$ is chosen when the Pantheon+ sample is utilized. We consider five expansion points (z_i) in redshift from 0.12 to 0.52 with an increment of 0.1 in our analysis. The number of SN Ia data in each redshift region is summarized in Table 1.

In Fig. 1, we show the constraints on $d_{L,i}$, H_i , and q_i from the Pantheon+ sample. The gray solid lines represent the evolutionary curves of $d_L(z)$, $H(z)$, and $q(z)$ in the Λ CDM model with $H_0 = 73.2 \pm 0.94 \text{ km s}^{-1} \text{ Mpc}^{-1}$ and $\Omega_{m0} = 0.33 \pm 0.018$, which are obtained from the Pantheon+ SN Ia data. To show the difference between these parameters and the predictions of the Λ CDM model clearly, we also plot $\Delta d_{L,i} \equiv d_{L,i} - d_{L,\Lambda\text{CDM}}$, $\Delta H_i \equiv H_i - H_{\Lambda\text{CDM}}$, and $\Delta q_i \equiv q_i - q_{\Lambda\text{CDM}}$. The uncertainties of $\Delta d_{L,i}$, ΔH_i , and Δq_i are calculated using the error propagation formula, *i.e.*, $\sigma_{\Delta d_{L,i}}^2 = \sigma_{d_{L,i}}^2 + \sigma_{d_{L,\Lambda\text{CDM}}}^2$, $\sigma_{\Delta H_i}^2 = \sigma_{H_i}^2 + \sigma_{H_{\Lambda\text{CDM}}}^2$, and $\sigma_{\Delta q_i}^2 = \sigma_{q_i}^2 + \sigma_{q_{\Lambda\text{CDM}}}^2$. Here, $\sigma_{d_{L,\Lambda\text{CDM}}}$, $\sigma_{H_{\Lambda\text{CDM}}}$, and $\sigma_{q_{\Lambda\text{CDM}}}$ represent the uncertainties derived from the Λ CDM model. The corresponding numerical results are summarized in Table 2. It is easy to see that all values of $d_{L,i}$ are compatible with the Λ CDM model. The values of H_i align with the Λ CDM model at the first three redshift points (*i.e.*, $z_i = 0.12, 0.22, \text{ and } 0.32$). However, they deviate from the model at the last two redshift points, with the largest deviation reaching about 1.8σ CL at $z_i = 0.42$. For the deceleration parameter, only the value at $z_i = 0.22$ slightly differs from the prediction of the model by about 1.3σ CL. We also plot the evolutionary curves of $d_L(z)$, $H(z)$, and $q(z)$ in the $w_0 w_a$ CDM model, shown as blue dashed lines in Fig. 1. For the $w_0 w_a$ CDM model, the EoS of dark energy is given by the CPL parametrization ($w_{\text{DE}} = w_0 + w_a \frac{z}{1+z}$). We set $H_0 = 72.98 \pm 0.94 \text{ km s}^{-1} \text{ Mpc}^{-1}$, $\Omega_{m0} = 0.282^{+0.160}_{-0.059}$, $w_0 = -0.91^{+0.18}_{-0.14}$ and $w_a = -0.28^{+1.40}_{-0.63}$, which are given by the Pantheon+ sample. One can see that most values of $d_{L,i}$, H_i , and q_i are consistent with the predictions of the $w_0 w_a$ CDM model. However, there are notable deviations: $d_{L,i}$ at $z_i = 0.52$ and H_i at $z_i = 0.42$ and 0.52 differ from this model by more than 1σ CL.

Using equation (4), we can derive the EoS parameter of dark energy at different redshifts ($w_{\text{DE},i}$) by considering the constraints on H_i and q_i . Setting $H_0 = 73.2 \pm 0.94 \text{ km s}^{-1} \text{ Mpc}^{-1}$ and $\Omega_{m0} = 0.33 \pm 0.018$, we obtain the values of $w_{\text{DE},i}$ at five different redshifts, which are shown in Fig. 2. We find that $w_{\text{DE},i}$ at $z_i = 0.22$ is slightly smaller than -1 , and other values of $w_{\text{DE},i}$ agree well with the -1 line within 1σ CL. Figure 2 shows that $w_{\text{DE},i}$ have very large uncertainties. This is because that only the SN Ia data in the redshift region $[z_i - \Delta z, z_i + \Delta z]$ are used and these SN Ia cannot provide tight constraints on H_i and q_i , especially q_i , which result in the large uncertainties on $w_{\text{DE},i}$.

3.2 P+1690 SN Ia

It is noteworthy that the Pantheon+ team employed the SALT2mu algorithm within the SNANA package (Kessler et al. 2009) to derive the corrected supernova sample, including the covariance matrix. This algorithm utilizes a fiducial cosmological model, specifically selecting the w CDM model for this purpose. Furthermore, the velocity field reconstruction (Carrick et al. 2015; Peterson et al. 2022), employed to adjust the redshift from z_{CMB} to z_{HD} within the Pantheon+ sample, also requires the use of a fiducial model. Although this dependency on the fiducial model has been observed to be weak (Carr et

al. 2022). Recently, an analysis of the Pantheon+ supernova catalog led to the creation of a truly cosmological-model-independent SN Ia sample Lane et al. (2023), comprising 1690 data points, referred to as the P+1690 sample in our study. Unlike the Pantheon+ sample, the P+1690 sample does not include bias corrections tied to any cosmological model, nor does its covariance matrix of light-curve parameters ($C_{\text{P+1690}}$) reflect uncertainties dependent on a cosmological model. Additionally, the P+1690 sample uses z_{CMB} rather than z_{HD} , thereby not relying on velocity field reconstruction.

To accommodate the P+1690 sample, which only provides the light-curve parameters $\{m_B, x_1, c\}$ with their covariance matrix $C_{\text{P+1690}}^\eta$, we need to adapt our calculation of the corrected distance modulus $\hat{\mu}_{\text{obs}}^{\text{corr}}$. This adjustment involves reformulating the relevant equations to work with the data format provided by the P+1690 sample (Betoule et al. 2014):

$$\hat{\mu}_{\text{obs}}^{\text{corr}} = \hat{A}\hat{\eta} + \hat{\delta}_{\text{host}} - M_B, \quad (8)$$

where the correction δ_{bias} is omitted. Here $\hat{A} = \hat{A}_0 + \alpha\hat{A}_1 - \beta\hat{A}_2$ with $(\hat{A}_k)_{i,j} \equiv \delta_{3i+k,j}$, and $\hat{\eta} = \{(m_B)_1, (x_1)_1, (c)_1, \dots, (m_B)_N, (x_1)_N, (c)_N\}$ is the one-dimension light-curve parameter vector of N data points and consists of $3 \times N$ elements. The $\hat{\delta}_{\text{host}}$ is a vector consisting of the following elements (Peterson et al. 2022):

$$\delta_{\text{host}} = \begin{cases} -\Delta_{\text{host}}, & \text{if } M_\star < 10^{10} M_\odot \\ +\Delta_{\text{host}}, & \text{if } M_\star \geq 10^{10} M_\odot. \end{cases} \quad (9)$$

Here M_\star and M_\odot are the host-galaxy mass and the solar mass, respectively, and Δ_{host} is a constant. The covariance matrix of the corrected distance modulus can be derived from

$$C_{\text{P+1690}} = \hat{A} C_{\text{P+1690}}^\eta \hat{A}^\dagger. \quad (10)$$

Replacing C_P with $C_{\text{P+1690}}$ in Eq. (5), we can obtain constraints on the cosmological parameters ($d_{L,i}$, H_i , q_i) from the P+1690 sample after setting $M_B = -19.253 \pm 0.027 \text{ mag}$ (Riess et al. 2022). In our analysis of the P+1690 sample, we consider the coefficients (α , β , Δ_{host}) as free parameters. To robustly account for their potential effects on the derived cosmological parameters, we simultaneously constrain these coefficients¹ and treat them as nuisance parameters through the marginalization method. Since the peculiar velocities can impact the SN Ia up to $z_{\text{CMB}} \approx 0.06$ (Davis et al. 2011), for the P+1690 sample, data with $z_{\text{CMB}} < 0.06$ are excluded in our discussions.

In Fig. 3, we show constraints on the parameters $d_{L,i}$, H_i , and q_i from the P+1690 sample. The black solid and blue dashed lines represent, respectively, the evolutions of $d_L(z)$, $H(z)$ and $q(z)$ in the Λ CDM model with $H_0 = 66.5 \pm 1.5 \text{ km s}^{-1} \text{ Mpc}^{-1}$ and $\Omega_{m0} = 0.356 \pm 0.032$, and the $w_0 w_a$ CDM model with $H_0 = 69.7 \pm 2.1 \text{ km s}^{-1} \text{ Mpc}^{-1}$, $\Omega_{m0} = 0.515^{+0.045}_{-0.018}$, $w_0 = -3.06^{+0.94}_{-0.75}$ and $w_a = 0.5^{+4.3}_{-2.5}$, which are given by the P+1690 sample. The corresponding numerical results are also summarized in the upper part of Table 3. It is easy to see that the allowed values of $d_{L,i}$ in the first three redshifts agree with the predictions of the Λ CDM model, while deviations from this model appear at more than 1σ CL for the last two redshift points (*i.e.*, $z_i = 0.42$ and 0.52). This result is different from that obtained from the Pantheon+ sample where it has been found that all values of $d_{L,i}$ are compatible with those derived

¹ In the MCMC analysis, we set the prior distribution of the coefficients (α , β , and Δ_{host}) to be uniform with ranges $0 \leq \alpha \leq 0.5$, $0 \leq \beta \leq 10$, and $-1 \leq \Delta_{\text{host}} \leq 1$, respectively, and obtain $\alpha = 0.217 \pm 0.008$, $\beta = 5.40^{+0.15}_{-0.17}$, and $\Delta_{\text{host}} = 0.031 \pm 0.006$ for the Λ CDM model.

Table 1. Number of data in each redshift range. The $N_{\text{Pantheon+}}$, $N_{\text{P+1690}}$ and $N_{H(z)}$ represent the number of Pantheon+ SN Ia data, P+1690 SN Ia data, and $H(z)$ data in each redshift range, respectively.

Redshift range	$z \leq 0.24^a$	$0.1 < z \leq 0.34$	$0.2 < z \leq 0.44$	$0.3 < z \leq 0.54$	$0.4 < z \leq 0.64$
$N_{\text{Pantheon+}}$	944	567	497	321	207
$N_{\text{P+1690}}$	378	566	493	317	206
$N_{H(z)}$	7	7	7	9	7

^a The data with $z < 0.01$ are excluded for the Pantheon+ sample, and with $z < 0.06$ are excluded for the P+1690 sample.

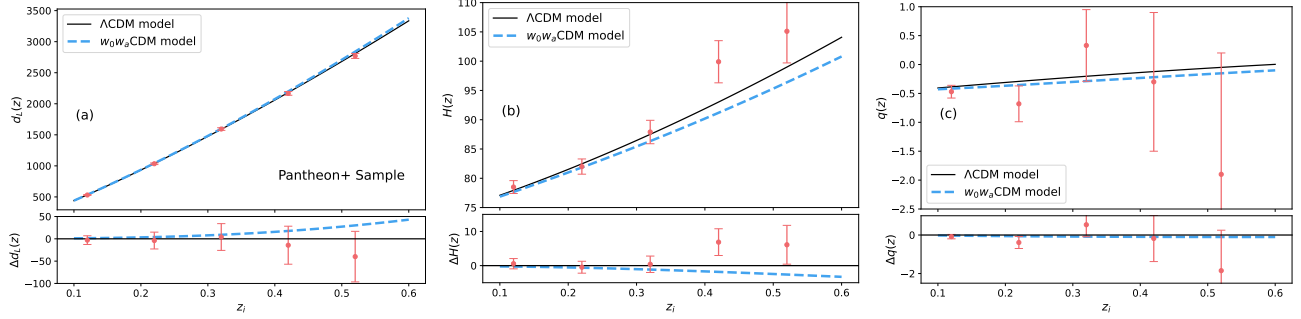


Figure 1. The constraints on $d_{L,i}$, H_i and q_i at different redshift points by using the Pantheon+ sample. The black solid and blue dashed lines represent, respectively, the predictions of the Λ CDM model with $H_0 = 73.2 \pm 0.94 \text{ km s}^{-1} \text{ Mpc}^{-1}$ and $\Omega_{m0} = 0.33 \pm 0.018$ and the w_0w_a CDM model with $H_0 = 72.98 \pm 0.94 \text{ km s}^{-1} \text{ Mpc}^{-1}$, $\Omega_{m0} = 0.282^{+0.160}_{-0.059}$, $w_0 = -0.91^{+0.18}_{-0.14}$ and $w_a = -0.28^{+1.40}_{-0.63}$. The symbol Δ denotes the differences between the results of $d_{L,i}$, H_i and q_i , and the predictions of Λ CDM model (solid line) and the w_0w_a CDM model (dashed line).

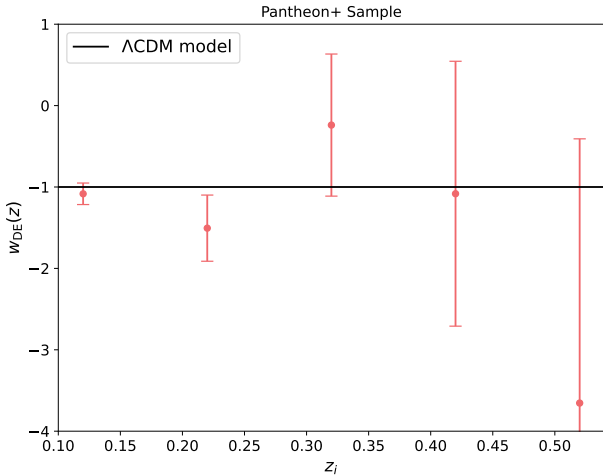


Figure 2. The values of $w_{\text{DE},i}$ derived from Eq. (4) with $H_0 = 73.2 \pm 0.94 \text{ km s}^{-1} \text{ Mpc}^{-1}$, $\Omega_{m0} = 0.33 \pm 0.018$ and the constraints on H_i and q_i from the Pantheon+ sample.

from the Λ CDM model. Moreover, the consistency between $d_{L,i}$ and the w_0w_a CDM model deteriorates when utilizing the P+1690 sample. For H_i , deviations from both the Λ CDM and w_0w_a CDM models are observed for the last three redshift points, contrary to the results shown in Fig. 1(b), with the greatest deviation at $z_i = 0.32$ reaching approximately 3σ CL. A deviation with similar statistical significance can also be observed in Fig. 3(c) where the constraints on q_i are plotted, and this deviation occurs at $z_i = 0.32$ too, which differs from those obtained from the Pantheon+ sample where the results are consistent with the Λ CDM model and the w_0w_a CDM model within 2σ CL.

Setting H_0 and Ω_{m0} to be $66.5 \pm 1.5 \text{ km s}^{-1} \text{ Mpc}^{-1}$ and 0.356 ± 0.032 , we derive the values of $w_{\text{DE},i}$ at five different redshifts, as shown in Fig. 4. We find that except for $z_i = 0.32$, all $w_{\text{DE},i}$ align within a 2σ CL of the expected $w_{\text{DE}} = -1$ value. The value of $w_{\text{DE},i}$ at $z_i = 0.32$ deviates from -1 by about 3σ CL, which is different from what is obtained from the Pantheon+ sample. Here, we must emphasize that the uncertainties of $w_{\text{DE},i}$ are quite high due to the lack of constraining data.

3.3 SN Ia plus $H(z)$ data

A prior fixed M_B may introduce some unknown bias in the results. To avoid this issue, we add the Hubble parameter measurements into our analysis and then M_B can be treated as a free parameter. The latest $H(z)$ data determined from the cosmic chronometric technique (Loeb 1998; Jimenez & Loeb 2002) comprises 32 data points, covering redshifts ranging from 0.07 to 1.965 (Simon et al. 2005; Stern et al. 2010; Moresco et al. 2012; Cong et al. 2014; Moresco 2015; Moresco et al. 2016; Ratsimbazafy et al. 2017; Borghi et al. 2022; Wu & Yu 2007). Here, we utilize only 19 data points that fall within the redshift range $z \leq 0.64$ (see Table 1 for details). To use the $H(z)$ data, we need to perform the Taylor expansion of the Hubble parameter similar to the equation (3):

$$H(z) = H_i \left(1 + (z - z_i) \frac{1 + q_i}{1 + z_i} \right) + O((z - z_i)^2). \quad (11)$$

The results from Pantheon+ plus $H(z)$ data are shown in Fig. 5 and the lower part of Table 2. This figure presents $d_{L,i}$, H_i , q_i , and the predicted $d_L(z)$, $H(z)$, $q(z)$ from the Λ CDM model with $H_0 = 67.5 \pm 1.7 \text{ km s}^{-1} \text{ Mpc}^{-1}$ and $\Omega_{m0} = 0.33 \pm 0.017$, and the w_0w_a CDM model with $H_0 = 67.5 \pm 1.8 \text{ km s}^{-1} \text{ Mpc}^{-1}$, $\Omega_{m0} = 0.320^{+0.095}_{-0.045}$, $w_0 = -0.93^{+0.12}_{-0.10}$ and $w_a = -0.47^{+1.4}_{-0.71}$, respectively. From Fig. 5(a), we find that, different from the results obtained

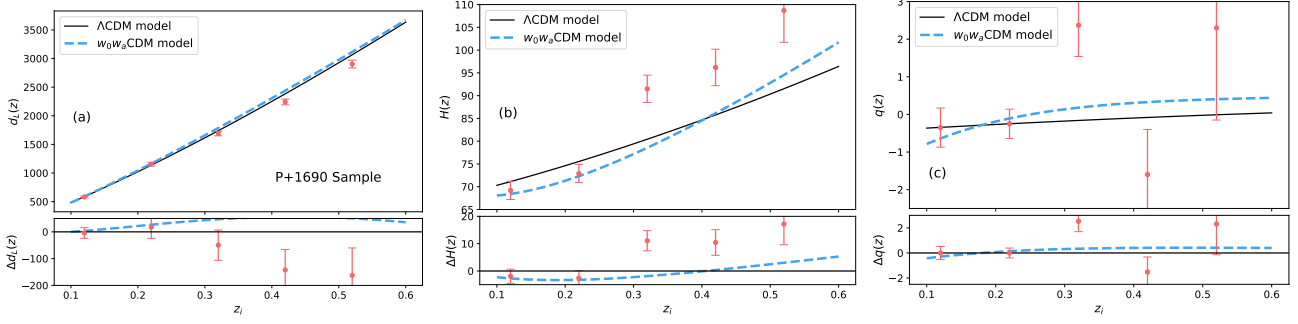


Figure 3. The constraints on $d_{L,i}$, H_i and q_i at different redshift points by using the P+1690 sample. The black solid and blue dashed lines represent, respectively, the predictions of the Λ CDM model with $H_0 = 66.5 \pm 1.5 \text{ km s}^{-1} \text{ Mpc}^{-1}$ and $\Omega_{m0} = 0.356 \pm 0.032$, and the $w_0 w_a$ CDM model with $H_0 = 69.7 \pm 2.1 \text{ km s}^{-1} \text{ Mpc}^{-1}$, $\Omega_{m0} = 0.515^{+0.045}_{-0.018}$, $w_0 = -3.06^{+0.94}_{-0.75}$ and $w_a = 0.5^{+4.3}_{-2.5}$. The symbol Δ denotes the differences between the results of $d_{L,i}$, H_i and q_i , and the predictions of the Λ CDM model (solid line) and the $w_0 w_a$ CDM model (dashed line).

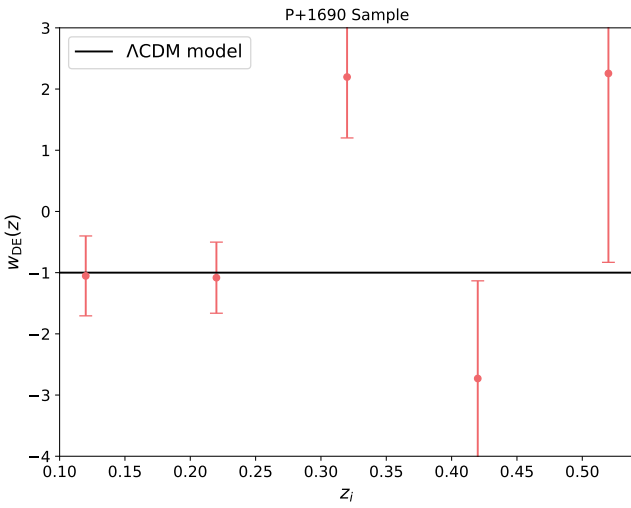


Figure 4. The values of $w_{\text{DE},i}$ derived from Eq. (4) with $H_0 = 66.5 \pm 1.5 \text{ km s}^{-1} \text{ Mpc}^{-1}$, $\Omega_{m0} = 0.356 \pm 0.032$ and the constraints on H_i and q_i from the P+1690 sample.

from the Pantheon+ only, the values of $d_{L,i}$ at $z_i = 0.42$ and 0.52 deviate from the Λ CDM model. Figure 5(b) indicates that the values of H_i are consistent with those from the Λ CDM model at 1σ CL, which are also different from the results obtained from Pantheon+ only. Similar to what are shown in Fig. 1, the value of q_i at $z_i = 0.22$ deviates from that from the Λ CDM model by about 1.3σ CL. However, the uncertainties of q_i are reduced significantly when the Hubble parameter measurements are included. For example, the 1σ uncertainty of q_i at $z_i = 0.52$ is reduced from 2.1 to 1.1 after adding the $H(z)$ data. This is expected since the parameter q_i appears in the first-order coefficient in the expansion of the Hubble parameter (Eq. (11)), making it more sensitive to q_i than Eq. (3). Thus, the SN Ia sample plus $H(z)$ data can provide tighter constraints on q_i than the SN Ia sample alone.

Figure 6 shows the values of $w_{\text{DE},i}$ after setting $H_0 = 67.5 \pm 1.7 \text{ km s}^{-1} \text{ Mpc}^{-1}$ and $\Omega_{m0} = 0.33 \pm 0.017$. One can see that except for the $w_{\text{DE},i}$ at $z_i = 0.22$ all other $w_{\text{DE},i}$ align with the -1 line within 1σ CL. This is similar to what are shown in Fig. 2.

Figure 7 and the lower part of Table 3 present constraints on the parameters obtained from the P+1690 sample plus $H(z)$ data. Their predicted values from the Λ CDM model with $H_0 = 67.0 \pm$

Table 2. Constraints on parameters in each redshift range using the Pantheon+ sample with and without the $H(z)$ data. The marginalized mean values with 1σ uncertainty of parameters are shown. Δ denotes the difference between the constraint results and the Λ CDM model.

Pantheon+ Sample				
z_i	$d_{L,i}$	H_i	q_i	$w_{\text{DE},i}$
0.12	531 ± 7	78.5 ± 1.1	-0.47 ± 0.11	-1.08 ± 0.13
0.22	1034 ± 13	82.0 ± 1.3	-0.68 ± 0.31	-1.51 ± 0.41
0.32	1593 ± 21	87.9 ± 2.0	0.33 ± 0.62	-0.24 ± 0.87
0.42	2167 ± 30	99.9 ± 3.6	-0.3 ± 1.20	-1.08 ± 1.63
0.52	2770 ± 40	105.1 ± 5.4	-1.90 ± 2.10	-3.65 ± 3.25
z_i	$\Delta d_{L,i}$	ΔH_i	Δq_i	$\Delta w_{\text{DE},i}$
0.12	-3 ± 10	0.6 ± 1.5	-0.08 ± 0.11	-0.08 ± 0.13
0.22	-4 ± 19	-0.5 ± 1.7	-0.39 ± 0.31	-0.50 ± 0.41
0.32	4 ± 30	0.4 ± 2.4	0.53 ± 0.62	0.76 ± 0.87
0.42	-14 ± 43	6.9 ± 3.9	-0.18 ± 1.20	-0.08 ± 1.63
0.52	-40 ± 57	6.1 ± 5.7	-1.85 ± 2.10	-2.65 ± 3.25
Pantheon+ Sample Plus $H(z)$ Data				
z_i	$d_{L,i}$	H_i	q_i	$w_{\text{DE},i}$
0.12	568 ± 20.5	73.4 ± 2.6	-0.47 ± 0.11	-1.06 ± 0.14
0.22	1108 ± 42	76.6 ± 2.9	-0.69 ± 0.31	-1.48 ± 0.41
0.32	1801 ± 130	78.1 ± 5.1	0.29 ± 0.55	-0.32 ± 0.85
0.42	2586 ± 155	83.7 ± 4.4	-0.4 ± 1.0	-1.56 ± 1.76
0.52	3354 ± 250	89.3 ± 6.5	0.0 ± 1.1	-0.99 ± 2.19
z_i	$\Delta d_{L,i}$	ΔH_i	Δq_i	$\Delta w_{\text{DE},i}$
0.12	-10.9 ± 25.2	1.5 ± 3.2	-0.08 ± 0.11	-0.06 ± 0.14
0.22	-18 ± 51	0.6 ± 3.5	-0.40 ± 0.31	-0.48 ± 0.41
0.32	78 ± 137	-2.6 ± 5.5	0.49 ± 0.55	0.68 ± 0.85
0.42	220 ± 166	-2.1 ± 5.0	-0.28 ± 1.00	-0.56 ± 1.76
0.52	307 ± 262	-2.0 ± 7.0	0.05 ± 1.10	0.01 ± 2.19

$2.0 \text{ km s}^{-1} \text{ Mpc}^{-1}$ and $\Omega_{m0} = 0.347 \pm 0.03$, and from the $w_0 w_a$ CDM model with $H_0 = 66.9 \pm 2.0 \text{ km s}^{-1} \text{ Mpc}^{-1}$, $\Omega_{m0} = 0.396^{+0.092}_{-0.048}$, $w_0 = -1.58^{+0.45}_{-0.26}$ and $w_a = 1.02^{+1.6}_{-0.59}$ are plotted as black solid and blue dashed lines, respectively. Contrary to the results obtained solely from P+1690 sample, the value of $d_{L,i}$ at $z_i = 0.32$ deviates from the predictions of the Λ CDM model by approximately 2σ CL. However, at $z_i = 0.52$, the value of $d_{L,i}$ aligns with the Λ CDM model, indicating consistency. Figure 7(b) indicates that H_i deviates from the predictions of the Λ CDM model only at $z_i = 0.32$. The constraints on deceleration parameter q_i are tighter than those obtained solely from P+1690 sample, but the value of q_i at $z_i = 0.32$ still deviates from that of the Λ CDM model by about 2.7σ CL. These results differ from those obtained from the Pantheon+ plus $H(z)$ data, in

Table 3. Constraints on parameters in each redshift range using the P+1690 sample with and without the $H(z)$ data. The marginalized mean values with 1σ uncertainty of parameters are shown. Δ denotes the difference between the constraint results and the Λ CDM model.

P+1690 Sample				
z_i	$d_{L,i}$	H_i	q_i	$w_{\text{DE},i}$
0.12	582 ± 15	69.2 ± 2.0	-0.35 ± 0.52	-1.05 ± 0.65
0.22	1155 ± 32	72.9 ± 2.0	-0.25 ± 0.39	-1.08 ± 0.58
0.32	1689 ± 39	91.5 ± 3.0	2.37 ± 0.83	2.20 ± 1.00
0.42	2241 ± 50	96.2 ± 4.0	-1.60 ± 1.20	-2.73 ± 1.60
0.52	2903 ± 68	108.7 ± 7.0	2.30 ± 2.45	2.26 ± 3.09
z_i	$\Delta d_{L,i}$	ΔH_i	Δq_i	$\Delta w_{\text{DE},i}$
0.12	-4 ± 20	-1.9 ± 2.6	-0.005 ± 0.523	-0.05 ± 0.65
0.22	17 ± 41	-2.6 ± 2.7	-0.001 ± 0.393	-0.08 ± 0.58
0.32	-50 ± 57	11.1 ± 3.7	2.53 ± 0.83	3.20 ± 1.00
0.42	-142 ± 77	10.4 ± 4.7	-1.52 ± 1.20	-1.73 ± 1.60
0.52	-163 ± 102	17.2 ± 7.6	2.31 ± 2.45	3.26 ± 3.09
P+1690 Sample Plus $H(z)$ Data				
z_i	$d_{L,i}$	H_i	q_i	$w_{\text{DE},i}$
0.12	552 ± 25	73.0 ± 3.2	-0.37 ± 0.49	-0.98 ± 0.56
0.22	1089 ± 41	77.3 ± 2.9	-0.26 ± 0.38	-0.96 ± 0.49
0.32	2098 ± 170	73.2 ± 5.2	1.94 ± 0.77	2.90 ± 1.86
0.42	2582 ± 165	83.9 ± 4.5	-1.40 ± 1.00	-3.46 ± 2.03
0.52	3319 ± 250	93.2 ± 6.4	1.04 ± 1.00	0.97 ± 1.82
z_i	$\Delta d_{L,i}$	ΔH_i	Δq_i	$\Delta w_{\text{DE},i}$
0.12	-30 ± 30	1.4 ± 3.9	-0.01 ± 0.49	0.02 ± 0.56
0.22	-42 ± 53	1.4 ± 3.8	0.003 ± 0.383	0.04 ± 0.49
0.32	369 ± 178	-7.5 ± 5.8	2.12 ± 0.77	3.90 ± 1.86
0.42	210 ± 181	-2.1 ± 5.4	-1.31 ± 1.00	-2.46 ± 2.03
0.52	267 ± 268	1.54 ± 7.20	1.06 ± 1.00	1.97 ± 1.82

which all constraints on $d_{L,i}$, H_i , and q_i are compatible with those from the Λ CDM model within 2σ CL. Furthermore, most of the constraints on $d_{L,i}$, H_i , and q_i are compatible with the predictions of the w_0w_a CDM model at 2σ CL. But q_i at $z_i = 0.32$ still shows a deviation of more than 2σ CL.

Figure 8 shows the values of $w_{\text{DE},i}$ after setting $H_0 = 67.0 \pm 2.0 \text{ km s}^{-1} \text{ Mpc}^{-1}$ and $\Omega_{\text{m}0} = 0.347 \pm 0.03$. Except for $w_{\text{DE},i}$ at $z_i = 0.32$, all values of $w_{\text{DE},i}$ align within a 2σ CL of $w_{\text{DE}} = -1$. These results are similar to those obtained using the P+1690 sample only.

Moreover, we find that the values of M_B obtained from both the Pantheon+ and P+1690 samples seem to decrease with the increase of redshift, as shown in the Table 4. To illustrate clearly this trend, we use a simple linear function: $M_B(z) = M_0 + \alpha z$ to fit the evolution of M_B , and obtain $M_0 = -19.31 \pm 0.11 \text{ mag}$ and $\alpha = -0.64 \pm 0.44 \text{ mag}$ for the Pantheon+ sample, and $M_0 = -19.05 \pm 0.15 \text{ mag}$ and $\alpha = -1.21 \pm 0.52 \text{ mag}$ for the P+1690 sample. Both M_0 are consistent with that obtained from the Cepheid host ($-19.253 \pm 0.027 \text{ mag}$) (Riess et al. 2022) within 2σ CL. However, the slope α deviates from zero by more than 2σ CL for the P+1690 sample. Note that a decreasing M_B with increasing redshift has also been observed in the Λ CDM model when combining SN Ia data with Hubble parameter measurements and baryonic acoustic oscillation data (Krishnan et al. 2020). This trend may be attributed to various astrophysical mechanisms (Hicken et al. 2009; Maoz et al. 2010; Kang et al. 2020), or it could suggest that the expansion of the universe does not strictly follow the average evolution predicted by the FLRW model (B & Suresh 2023; Akarsu et al. 2024). Furthermore, due to the degeneracy between Hubble constant H_0 and M_B , this trend could also be influenced by variations

Table 4. Constraints on M_B obtained from the Pantheon+ and P+1690 samples plus the $H(z)$ data.

z_i	Pantheon+ Sample	P+1690 Sample
0.12	-19.40 ± 0.08	-19.14 ± 0.11
0.22	-19.40 ± 0.08	-19.20 ± 0.01
0.32	-19.52 ± 0.16	-19.72 ± 0.18
0.42	-19.63 ± 0.13	-19.55 ± 0.15
0.52	-19.65 ± 0.17	-19.54 ± 0.18

in H_0 , as observed in several studies (Wong et al. 2020; Dainotti et al. 2021; Hu & Wang 2022).

4 CONCLUSIONS

To determine whether the cosmic evolution is consistent with the predictions of the Λ CDM model, we establish a new and cosmological-model-independent method to explore the cosmic dynamics from observational data. Using the Pantheon+ sample and a model-independent P+1690 SN Ia sample, we obtain the values of $d_{L,i}$, H_i and q_i at five different redshift points, and calculate the EoS of dark energy $w_{\text{DE},i}$ at these redshifts. We find that all results obtained from the Pantheon+ sample are consistent with the predictions of the Λ CDM model within 2σ CL. However, the constraints on H_i from the P+1690 sample deviate from the predictions of the Λ CDM model at $z_i = 0.32, 0.42$, and 0.52 by more than 2σ CL, with the largest deviation reaching about 3σ CL. A similar deviation is also observed in the result for q_i at $z_i = 0.32$. Moreover, the EoS of dark energy obtained from the P+1690 sample also deviates from the -1 line by about 3σ CL. After further considering the Hubble parameter measurements, we find that q_i and $w_{\text{DE},i}$ still deviate from the predictions of the Λ CDM model at $z_i = 0.32$ by about 3σ CL, although the constraints on H_i become consistent with the model within 2σ CL. We also find that a linearly decreasing absolute magnitude of SN Ia with the increase of redshift is favored, as the slope of the linear function deviates from zero by more than 1σ CL. Our results show that the Λ CDM model remains compatible with the Pantheon+ SN Ia and the Hubble parameter measurements within 2σ CL, but only within 3σ CL for the P+1690 sample.

ACKNOWLEDGMENTS

This work was supported in part by the NSFC under Grant Nos. 12275080 and 12075084 and the innovative research group of Hunan Province under Grant No. 2024JJ1006.

DATA AVAILABILITY

Data are available at the following references: the Pantheon+ SNe Ia sample from Scolnic et al. (2022), the P+1690 sample from Lane et al. (2023), and the latest $H(z)$ data obtained with the CC method from Cao & Ratra (2022).

REFERENCES

- Abbott, T. M. C., Acevedo, M., Aguena, M., et al. 2024, [arXiv:2401.02929](https://arxiv.org/abs/2401.02929)
 Akarsu, Ö., Colgáin, E. Ó., Sen, A. A., & Sheikh-Jabbari, M. M. 2024, [arXiv:2402.04767](https://arxiv.org/abs/2402.04767)

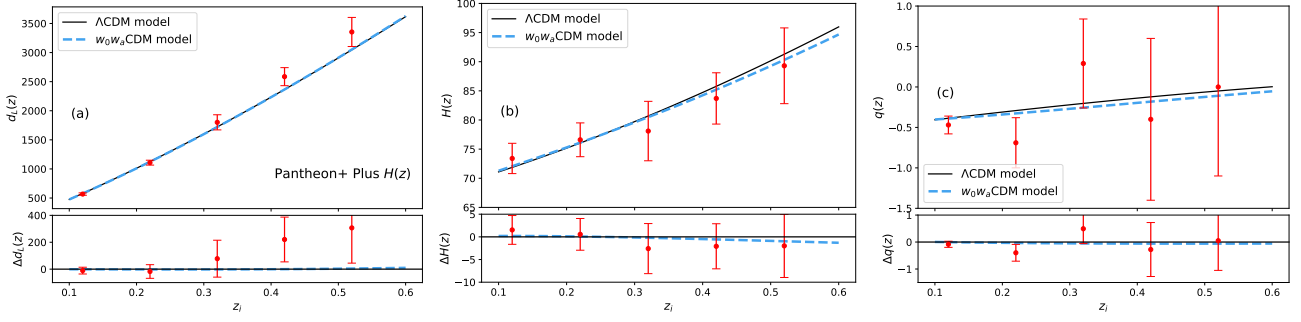


Figure 5. The constraints on $d_{L,i}$, H_i and q_i at different redshift points by using the Pantheon+ sample plus $H(z)$ data. The black solid and blue dashed lines represent, respectively, the predictions of the Λ CDM model with $H_0 = 67.5 \pm 1.7 \text{ km s}^{-1} \text{ Mpc}^{-1}$ and $\Omega_{m0} = 0.33 \pm 0.017$, and the w_0w_a CDM model with $H_0 = 67.5 \pm 1.8 \text{ km s}^{-1} \text{ Mpc}^{-1}$, $\Omega_{m0} = 0.320^{+0.095}_{-0.045}$, $w_0 = -0.93^{+0.12}_{-0.10}$ and $w_a = -0.47^{+1.4}_{-0.71}$. The symbol Δ denotes the differences between the results of $d_{L,i}$, H_i and q_i , and the predictions of the Λ CDM model (solid line) and the w_0w_a CDM model (dashed line).

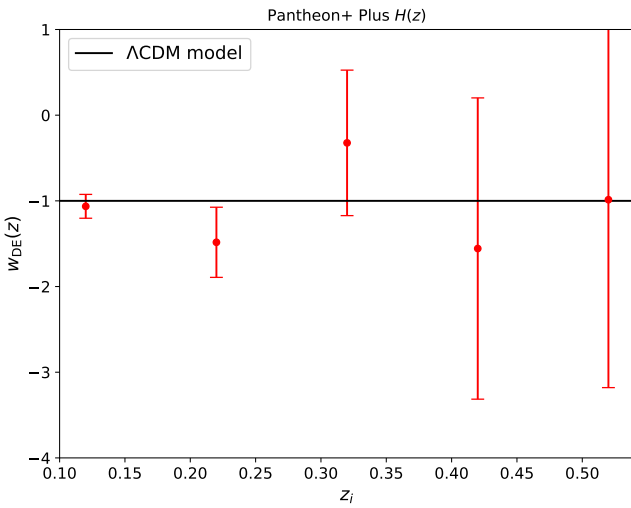


Figure 6. The values of $w_{DE,i}$ derived from Eq. (4) with $H_0 = 67.5 \pm 1.7 \text{ km s}^{-1} \text{ Mpc}^{-1}$, $\Omega_{m0} = 0.33 \pm 0.017$ and the constraints on H_i and q_i from the Pantheon+ sample plus $H(z)$ data.

- Aviles, A., Gruber, C., Luongo, O., & Quevedo, H. 2012, *Phys. Rev. D*, **86**, 123516
- B, Anupama & Suresh, P. K. 2023, *Class. Quant. Grav.*, **41** 035002
- Betoule, M., Kessler, R., Guy, J., et al. 2014, *A&A*, **568**, A22
- Brout, D., & Scolnic, D. 2021, *ApJ*, **909**, 26
- Brout, D., Scolnic, D., Popovic, B., et al. 2022, *ApJ*, **938**, 110
- Borghini, N., Moresco, M., & Cimatti, A. 2022, *ApJ*, **928**, L4
- Cao, S., & Ratra, B. 2022, *MNRAS*, **513**, 5686
- Capozziello, S., D'Agostino, R., & Luongo, O. 2019, *IJMPD*, **28**, 1930016
- Capozziello, S., D'Agostino, R., & Luongo, O. 2020, *MNRAS*, **494**, 2576
- Carr, A., Davis, T. M., Scolnic, D., et al. 2022, *Publ. Astron. Soc. Australia*, **39**, e046
- Carron, J., Mirmelstein, M., & Lewis, A. 2022, *J. Cosmology Astropart. Phys.*, **09**, 039
- Carrick, J., Turnbull, S. J., Lavaux, G., & Hudson, M. J. 2015, *MNRAS*, **450**, 317
- Cardona, W., Kunz, M., & Pettorino, V. 2017, *J. Cosmology Astropart. Phys.*, **03**, 056
- Chevallier, M., & Polarski, D. 2001, *IJMPD*, **10**, 213
- Cong, Z., Han, Z., Shuo, Y., et al. 2014, *Res. Astron. Astrophys.*, **14**, 1221
- Dainotti, M. G., Simone, B. D., Schiavone, T., et al. 2021, *ApJ*, **912**, 150
- Davis, T. M., Hui, L., Frieman J. A., et al. 2011, *ApJ*, **741**, 67
- DESI Collaboration, 2024, *arXiv:2404.03002*
- Demianski, M., Lusso, E., Paolillo, M., Piedipalumbo, E., Risaliti, G. 2020, *Front. Astron. Space Sci.*, **7**, 69
- Dunsby, P. K. S., & Luongo, O. 2016, *IJGMMP*, **13**, 1630002
- Efstathiou, G. 2014, *MNRAS*, **400**, 1138
- Feeney, S. M., Mortlock, D. J., & Dalmasso, N. 2018, *MNRAS*, **476**, 3861
- Follin, B., & Knox, L. 2018, *MNRAS*, **477**, 4534
- Gao, J., Zhou, Z., Du, M., et al. 2023, *arXiv:2307.08285*
- Hicken, M., Wood-Vasey, W. M., Blondin, S., et al. 2009, *ApJ*, **700**, 1097
- Holsclaw, T., Alam, U., Sansó, B., et al. 2010, *Phys. Rev. Lett.*, **105**, 241302
- Hu, J. P., & Wang, F. Y. 2022, *MNRAS*, **517**, 576
- Jimenez, R., & Loeb, A. 2002, *ApJ*, **573**, 37
- Kessler, R., Bernstein, J. P., Cinabro, D., et al., 2009, *PASP*, **121**, 1028
- Krishnan, C., Colgáin, E. Ó., Ruchika, et al. 2020, *Phys. Rev. D*, **102**, 103525
- Lane, Z. G., Seifert, A., Ridden-Harper, R., Wagner, J., Wiltshire, D. L. 2023, *arXiv:2311.01438*
- Linder, E. V. 2003, *Phys. Rev. Lett.*, **90**, 091301
- Liu, D.-J., Li, X.-Z., Hao, J., & Jin, X.-H. 2008, *MNRAS*, **388**, 275
- Liu, Y., Yu, H., & Wu, P. 2023, *ApJ*, **946**, L49
- Liu, Y., Yu, H., & Wu, P. 2024, *arXiv: 2406.02956*
- Loeb, A. 1998, *ApJ*, **499**, L111
- Luongo, O. 2011, *Mod. Phys. Lett. A*, **26**, 1459
- Maoz, D., Sharon, K., & Gal-Yam, A. 2010, *ApJ*, **722**, 1879
- Mehrabi, A., & Rezaei, M. 2021, *ApJ*, **923**, 274
- Moresco, M., Cimatti, A., Jimenez, R., et al. 2012, *J. Cosmology Astropart. Phys.*, **08**, 006
- Moresco, M. 2015, *MNRAS Lett.*, **450**, L16
- Moresco, M., Pozzetti, L., Cimatti, A., et al. 2016, *J. Cosmology Astropart. Phys.*, **05**, 014
- Peterson, E. R., Kenworthy, W. D., Scolnic, D., et al. 2022, *ApJ*, **938**, 112
- Perivolaropoulos, L., & Skara, F. 2022, *New Astron. Rev.*, **95**, 101659
- Planck Collaboration, 2020, *A&A*, **641**, A6
- Planck Collaboration, 2020, *A&A*, **641**, A5
- Popovic, B., Brout, D., Kessler, R., Scolnic, D., & Lu, L. 2021, *ApJ*, **913**, 49
- Qu, F. J., Sherwin, B. D., Madhavacheril, M. S., et al. 2024, *ApJ*, **962**, 112
- Ratsimbazafy, A. L., Loubser, S. I., Crawford, S. M., et al. 2017, *MNRAS*, **467**, 3239
- Riess, A. G. 2020, *Nat. Rev. Phys.*, **2**, 10
- Riess, A. G., Yuan, W., Macri, L. M., et al. 2022, *ApJ*, **934**, L7
- Riess, A. G., Macri, L. M., Hoffmann, S. L., et al. 2016, *ApJ*, **826**, 56
- Riess, A. G., Casertano, S., Yuan, W., et al. 2018, *ApJ*, **855**, 136
- Riess, A. G., Casertano, S., Yuan, W., et al. 2018, *ApJ*, **861**, 126
- Scolnic, D., Brout, D., Carr, A., et al. 2022, *ApJ*, **938**, 113
- Seikel, M., Clarkson, C., & Smith, M. 2012, *J. Cosmology Astropart. Phys.*, **06**, 036
- Shafieloo, A., Kim, A. G., & Linder, E. V. 2012, *Phys. Rev. D*, **85**, 123530
- Simon, J., Verde, L., & Jimenez, R. 2005, *Phys. Rev. D*, **71**, 123001
- Stern, D., Jimenez, R., Verde, L., et al. 2010, *J. Cosmology Astropart. Phys.*, **02**, 008
- Tripp R., 1998, *A&A*, **331**, 815

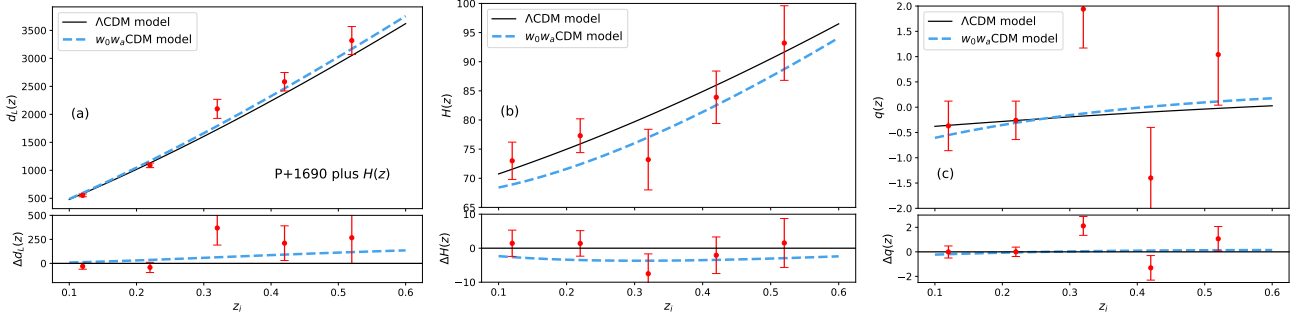


Figure 7. The constraints on $d_{L,i}$, H_i and q_i at different redshift points by using the P+1690 sample plus $H(z)$ data. The black solid and blue dashed lines represent, respectively, the predictions of the Λ CDM model with $H_0 = 67.0 \pm 2.0 \text{ km s}^{-1} \text{ Mpc}^{-1}$ and $\Omega_{m0} = 0.347 \pm 0.03$, and the w_0w_a CDM model with $H_0 = 66.9 \pm 2.0 \text{ km s}^{-1} \text{ Mpc}^{-1}$, $\Omega_{m0} = 0.396^{+0.092}_{-0.048}$, $w_0 = -1.58^{+0.45}_{-0.26}$ and $w_a = 1.02^{+1.6}_{-0.59}$. The symbol Δ denotes the differences between the results of $d_{L,i}$, H_i and q_i , and the predictions of Λ CDM model (solid line) and the w_0w_a CDM model (dashed line).

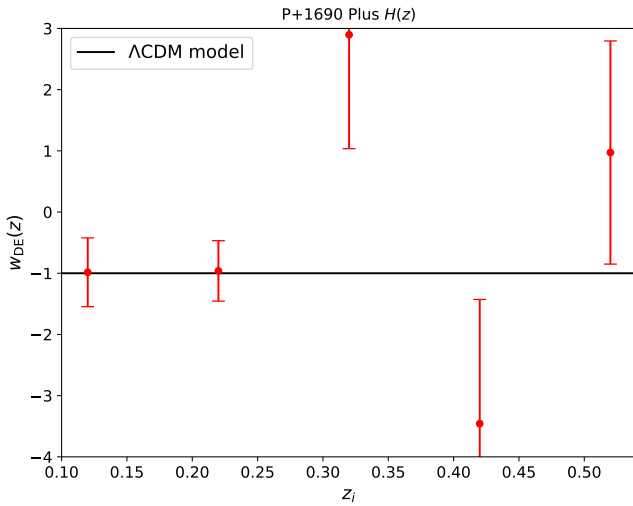


Figure 8. The values of $w_{DE,i}$ derived from Eq. (4) with $H_0 = 67.0 \pm 2.0 \text{ km s}^{-1} \text{ Mpc}^{-1}$, $\Omega_{m0} = 0.347 \pm 0.03$ and the constraints on H_i and q_i from the P+1690 sample plus $H(z)$ data.

Tully, R. B. [arXiv:2305.11950](https://arxiv.org/abs/2305.11950).

Visser, M. 2005, *Gen. Relativ. Gravit.*, 37, 1541

Wong, K. C., Suyu, S. H., Chen, G. C-F., et al. 2020, *MNRAS*, 498, 1420

Wu, P & Yu, H. 2007, *Phys. Lett. B* 644, 16

Kang, Y., Lee, Y-W., Kim, Y-L., Chung, C., & Ree, C. H. 2020, *ApJ*, 889, 8

Zhang, B. R., Childress, M. J., Davis, T. M., et al. 2017, *MNRAS*, 471, 2254

Zhang, K., Zhou, T., Xu, B., Huang, Q., & Yuan, Y. 2023, *ApJ*, 957, 5

Zhao, G. B., Crittenden, R. G., Pogossian, L., & Zhang, X. 2012, *Phys.*

Rev. Lett., 109, 171301

Zhao, G. B., Raveri, M., Pogossian, L., et al. 2017, *Nat. Astron.*, 1, 627

APPENDIX A: CHECKING THE RELIABILITY OF OUR METHOD

To determine the impact of the choice of different Δz on the constraints of the parameters $d_{L,i}$, H_i , and q_i in Sec. II, we plan to simulate the SN Ia data to constrain these parameters. We firstly employ the Kernel Density Estimate (KDE) with a band width $b = 0.01$ to describe the redshift distribution of the Pantheon+ sample, and use this redshift distribution to sample randomly 1590 points in the redshift region over $0.01 < z \leq 2.26$, which is the same as that of

the Pantheon+ sample. At each redshift point, the value of theoretical apparent magnitude $\langle m_{\text{th}} \rangle$ can be calculated from $m_{\text{th}} = \mu_{\text{th}} + M_B$ by assuming a fiducial model: the flat Λ CDM model with $\Omega_{m0} = 0.33$, $H_0 = 73.2 \text{ km s}^{-1} \text{ Mpc}^{-1}$, and $M_B = -19.253 \text{ mag}$, which are obtained from the Pantheon+ sample. Then, the mock m_{sim} can be sampled from the Gaussian distribution $\mathcal{N}(\langle m_{\text{th}} \rangle, \sigma_{\text{SN}})$. Here σ_{SN} is the uncertainty of $\langle m_{\text{th}} \rangle$, which is obtained from the Pantheon+ sample. From these mock SN Ia data, the parameters ($d_{L,i}$, H_i , and q_i) can be estimated by using the minimum χ^2 method (equation (5)), and $\Delta d_{L,i} \equiv d_{L,i} - d_{L,\text{th}}$, $\Delta H_i \equiv H_i - H_{\text{th}}$ and $\Delta q_i \equiv q_i - q_{\text{th}}$ at each redshift point can also be calculated, where the subscript ‘th’ denotes the prediction from the fiducial model. After repeating above process 1000 times, we plot the distributions of the deviations $\Delta d_{L,i}$, ΔH_i , and Δq_i . If these 1000 deviations are concentrated around zero line, it implies that our method does not introduce any unknown errors and is reliable.

Here we consider two different cases: choosing $\Delta z = 0.12$ and $\Delta z = 0.15$, respectively. The redshift expansion points z_i are (0.12, 0.22, 0.32, 0.42, 0.52) and (0.15, 0.25, 0.35, 0.45, 0.55) for the first and second cases, respectively. The redshift points at $z_i > 0.6$ are also calculated but the results are not shown in the paper since the constraints on the cosmological parameters are weak due to that the data points in the Δz range are too few. Fig. A1 and A2 show the results of two cases with different redshift points, respectively. For both cases, it is easy to see that all results are compatible with the fiducial model at the 1σ CL. However, in the case of $\Delta z = 0.15$, $\Delta q_1 = 0$ is consistent with the mean of 1000 Δq_1 only at the margin of 1σ confidence level. Thus, we choose $\Delta z = 0.12$ in our analysis.

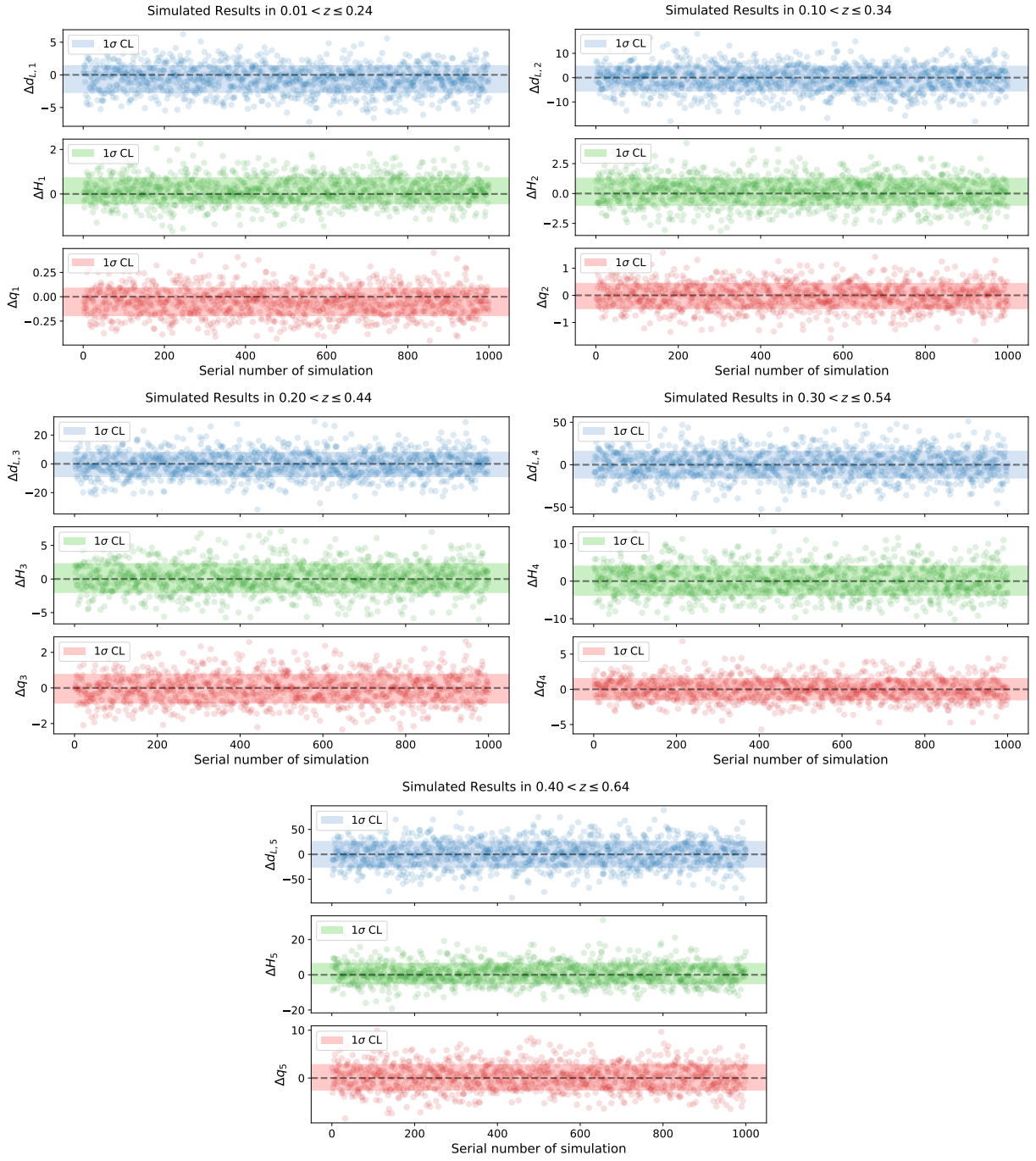


Figure A1. The distribution of $\Delta d_{L,i}$, ΔH_i , and Δq_i from 1000 time simulated data in the case of $\Delta z = 0.12$. The shadow shows the 1σ uncertainty.

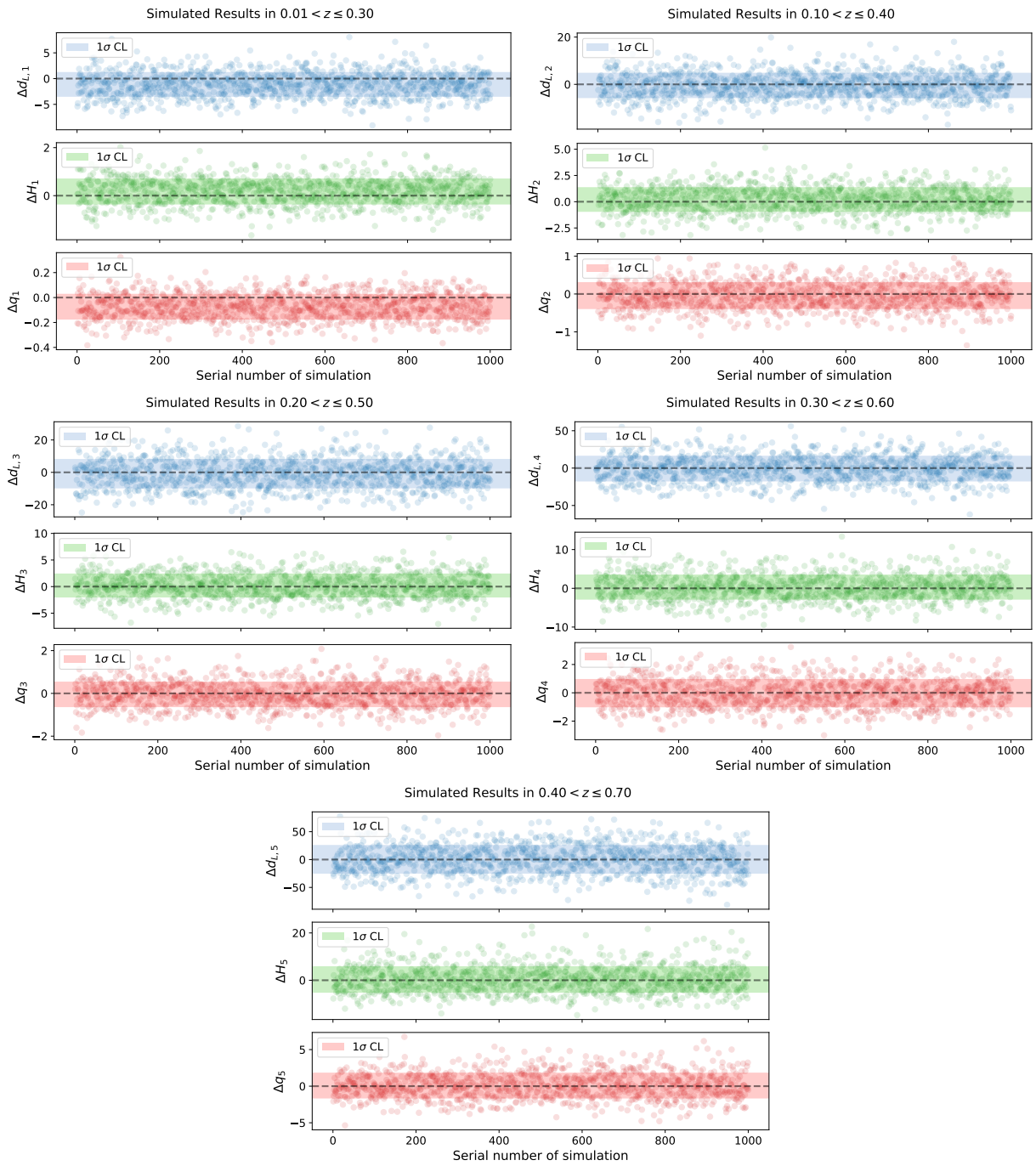


Figure A2. The distribution of $\Delta d_{L,i}$, ΔH_i , and Δq_i from 1000 time simulated data in the case of $\Delta z = 0.15$. The shadow shows the 1σ uncertainty.